Available online at www.sciencedirect.com
SCIENCE DIRECT®
International Journal of Heat and Mass Transfer 48 (2005) 1825–1839
International Journal of HEAT and MASS TRANSFER
www.elsevier.com/locate/ijhmt

Calculation of dry out and post-dry out heat transfer in rod bundles using a three field model

Sreenivas Jayanti [1], Michel Valette *

CEA-Grenoble DER/SSTH, 17 rue des Martyrs, 38054 Grenoble Cedex 9, France

Received 24 July 2004; received in revised form 8 November 2004
Available online 22 December 2004

Abstract

The critical heat flux (CHF) condition is an important parameter in the design and operation of nuclear reactor fuel rod assemblies. It has traditionally been evaluated using look-up tables or empirical correlations. In the present paper, a set of relations, in the form of a one-dimensional three-field model, is presented which enables a mechanistic prediction of high-quality CHF known as dry out. This also allows a more fundamental treatment of post-dry out heat transfer. The ensemble of relations is validated by comparing the predictions with data obtained from the TPTF test series of JAERI and the THTF test series of ORNL. The rod bundles have been modelled on a sub-channel basis. The effect of spacer grids on the flow and heat transfer has been studied by including their geometrical characteristics only. Good predictions of the dry out location and the post-dry out variation of the rod temperature are obtained over the range of parameters investigated in these tests, namely, in the pressure range of 30–130 bar, mass flux range of 50–800 kg/m^2 s and inlet condition ranging from sub-cooled to an inlet quality of 0.89.

1. Introduction

The critical heat flux (CHF) condition is an important parameter in the design and operation of nuclear reactor fuel rod assemblies. It is the condition in which the tube wall is not wetted by the liquid and is in direct contact with the vapour phase. The resulting deterioration of the convective boiling heat transfer mechanism results in a large rise in the wall temperature in a heat flux imposed system such as a nuclear reactor. The wall temperature in post-CHF conditions is a key parameter of safety analysis of nuclear reactor systems and the calculation of CHF and post-CHF heat transfer is therefore of paramount importance. Two generic mechanisms of CHF are usually distinguished (Collier, [1]): CHF occurring at under subcooled or low quality conditions and that occurring in annular flow at high qualities. The latter (also known as dry out) is a result of progressive loss of liquid from the liquid film due to entrainment and evaporation and is considered as an operating limit in nuclear reactors. Traditional approaches to the prediction of critical heat flux are purely empirical in which look-up tables [2,3] and empirical correlations [4,5] are used to calculate the CHF for a given condition. Both these approaches are still being used [6–9] with updated tables and correlations as they offer perhaps the most cost-effective way of determining CHF. However, these approaches have

* Corresponding author. Tel.: +33 4 38 79 55 37; fax: +33 4 38 78 51 95.
E-mail addresses: sjayanti@iitm.ac.in (S. Jayanti), michel.valette@cea.fr (M. Valette).
[1] On leave from IIT, Madras, India.

0017-9310/$ - see front matter © 2004 Elsevier Ltd. All rights reserved.
doi:10.1016/j.ijheatmasstransfer.2004.11.005

Nomenclature

A	flow cross section area (m^2)
C_d	drag coefficient of droplets in gas
D_h	pipe hydraulic diameter (m)
f_i	friction coefficient at interface
g	acceleration due to gravity ($m\ s^{-2}$)
H	specific enthalpy (J/kg)
k_d	droplet deposition coefficient ($m\ s^{-1}$)
k_q	droplet deposition inhibition coefficient ($m\ s^{-1}$)
k_s	equivalent sand grain roughness height (m)
$\dot{m}_{lfc}$	critical liquid film mass velocity ($kg\ m^{-2}\ s$)
P	static pressure (Pa)
p_{ilcg}	pressure at the interface between continuous liquid and gas (Pa)
p_{ildg}	pressure at the interface between dispersed liquid and gas (Pa)
q	heat flux
q_{lci}	heat transfer rate per unit volume between continuous liquid and its interface with gas (W/m^3)
q_{ldi}	heat transfer rate per unit volume between dispersed liquid and its interface with gas (W/m^3)
q_{vic}	heat transfer rate per unit volume between gas and interface with continuous liquid (W/m^3)
q_{vid}	heat transfer rate per unit volume between gas and interface with dispersed liquid (W/m^3)
q_{wlc}	heat transfer rate per unit wall contact area between wall and continuous liquid (W/m^2)
q_{wld}	heat transfer rate per unit wall contact area between wall and dispersed liquid (W/m^2)
q_{wv}	heat transfer rate per unit wall contact area between wall and gas (W/m^2)
q_{wic}	heat flux per unit interfacial area between wall and the gas/continuous liquid interface (W/m^2)
q_{wid}	heat flux per unit interfacial area between wall and the gas/dispersed liquid interface (W/m^2)
R	stratification ratio
Re	Reynolds number
t	time (s)
T	temperature (C)
V	phase-averaged velocity ($m\ s^{-1}$)
W_{icv}	interface velocity between continuous liquid and gas ($m\ s^{-1}$)
W_{idv}	interface velocity between dispersed liquid and gas ($m\ s^{-1}$)
z	axial coordinate (m)

Greek symbols

α	volume fraction of phase
β	added mass coefficient
Γ	mass transfer rate between two phases ($kg\ m^{-3}\ s^{-1}$)
Γ_a	droplet entrainment rate ($kg\ m^{-3}\ s^{-1}$)
Γ_d	droplet deposition rate ($kg\ m^{-3}\ s^{-1}$)
Γ_{lcv}	evaporation rate from continuous liquid ($kg\ m^{-3}\ s^{-1}$)
δ	droplet diameter (m)
μ	dynamic viscosity ($kg\ m^{-1}\ s^{-1}$)
ρ	density ($kg\ m^{-3}$)
σ	surface tension ($N\ m^{-1}$)
τ	shear stress (Pa)
τ_{icv}	interfacial shear force per unit volume between continuous liquid and gas (N/m^3)
τ_{idv}	interfacial shear force per unit volume between dispersed liquid and gas (N/m^3)
χ_f	wetted perimeter (m)
χ_h	heated perimeter based on wall contact area (m)

Subscripts

a	related to droplet entrainment
b	related to boiling
d	related to deposition of droplets
g	related to gas
i	related to interface
k	related to phase k
lc	related to continuous liquid
ld	related to dispersed liquid
sat	related to saturated liquid condition
v	related to vapour or gas
w	related to wall

limited applicability outside the range of parameters and also cannot take account of case-specific features such as the presence of obstacles, adiabatic regions, change in cross-section etc. An alternative, more physical approach to the prediction of dry out was pioneered at the United Kingdom Atomic Energy Authority (UKAEA) in which a ''phenomenological'' model is used for the prediction of dry out based on mass balance equations [10] incorporating empirical correlations for the underlying hydrodynamic processes of entrainment and deposition of droplets [11,1]. Later studies extended this to include thermal non-equilibrium conditions and to a wider range of flow conditions including transient flow situations in tubes, annuli and rod bundles for pressures up to 70 bar for a steam-water system [12]. A more recent development in the prediction methodology is the

use of two-phase, three-fluid models in which the full set of conservation equations (mass, momentum and energy conservation equations) are solved for three fields, namely, the liquid film, the liquid droplets and the vapour. The solution of the conservation equations for the droplet field enables a phenomenological prediction of the post-dry out heat transfer in addition to the prediction of dry out. The prediction of the droplet field is also important in the calculation of rewetting in the context of the loss-of-coolant accident (LOCA) scenarios in nuclear reactors. The set of these fundamental and constitutive relations is incorporated in computer codes such as FIDAS [13], MONA [14], COBRA-TF [15], NEPTUNE [16]. In a recent work [17], the present authors reported a new set of constitutive relations to extend the range of application to up to 200 bar for steam-water flow through tubes.

Thus, there is considerable literature on the prediction of dry out in flow through tubes. In contrast, much less work has been reported for the more practical case of rod bundles in which the fluid flows in the interstices between heated rods, typically of 10 mm diameter. Empirical correlations developed for flow inside tubes tend to overpredict the CHF, sometimes by a large margin [6], in rod bundles. This is not surprising because rod bundles bring in a number of effects which are not present in CHF in single tubes: flow non-uniformities across the tube bundles, non-uniformity of heat flux, radial mixing, effect of internal features such as twisted tapes and spacer grids, and, at a more fundamental level, flow through non-circular cross-section, partially heated perimeter, and the film flow on the outside of a tube rather than on the inside of a tube. A number of these factors have been included as correction factors in the CHF look-up tables [3,18,19]. At a more fundamental level, experiments have also been conducted in annuli [20,21] to simulate the effect of flow through tubes of non-circular geometry. It is thought that for films which are very thin compared to the radii of the annulus, the entrainment rates from the inner and outer films of an annulus are not very different. Studies of CHF in rod bundles using two-fluid models [22,23] and multi-fluid models [24–26,13] have also been reported in the literature. Two-fluid models use either an empirical correlation or a look-up table to determine CHF. In the multi-field models, wherein separate conservation equations are solved for the droplet phase, the correlations used for droplet entrainment and redeposition remain the same as those used for flow through single tubes. The calculations are done on a sub-channel basis. Additional models are incorporated to account for spacer grid effects. The overall model in each case has been compared with a limited amount of data. Knabe and Wehle [25] and Naitoh et al. [13] compared predictions of the critical power for typical boiling water reactor (BWR) applications but did not deal with post-dry out heat transfer. Sugawara and Miyamoto [24] conducted extensive validation for the prediction of dry out but presented only limited assessment of the post-dry heat transfer in the form of time history of the wall temperature in a rod bundle during power transients. Hoyer and Stepniewski [26] extended the model of Hoyer [14] for flow inside a tube to a rod bundle and showed model capabilities for typical BWR power transients.

Thus, while a lot of progress has been made in the prediction of dry out in a rod bundle on a mechanistic basis, the post-dry out heat transfer has not been systematically addressed. Also, while specific models for spacer grids have been used in all studies, the effect of these on CHF and post-CHF conditions has not been brought out clearly. For example, the effect of spacer grids is clearly evident in the data from the Thermal Hydraulic Test Facility (THTF) of ORNL, Tennessee,

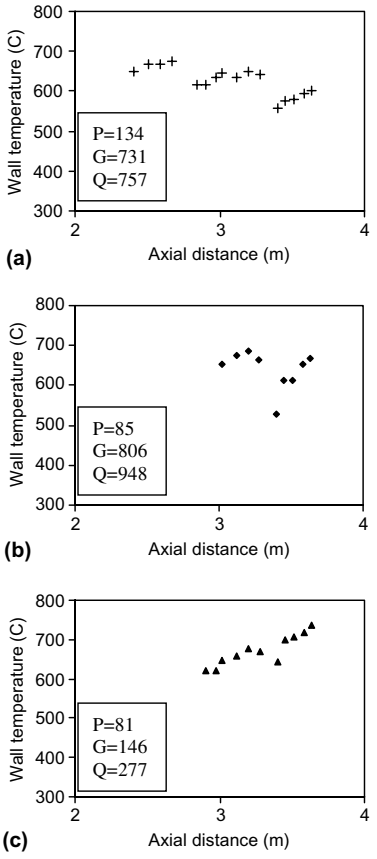

Fig. 1. Data taken from the THTF test series [27] illustrating the effect of spacer grids on the post-dry out wall temperature variation in an 8×8 rod bundle: (a) Case J, (b) Case N, and (c) Case ID. The pressure P (in bar), mass flux G (in kg/m^2 s) and heat flux Q (in kW/m^2) are indicated in each figure.

USA, [27]. Here, the surface wall temperature was measured in a well-instrumented 8×8 rod bundle of a typical pressurized water reactor (PWR) assembly under steady state conditions. The average wall temperature of the rods measured under steady flow conditions for three different tests, namely, tests J, N and ID are plotted in Fig. 1 as a function of axial distance. These show that, typically, the wall temperature in the post-dry out region exhibits a sudden fall and a rapid rise around the spacers. The extent of the temperature discontinuity and the rapidity of the recovery depend on flow conditions. In the present paper, these THTF data and those obtained [6,28] from the Two-Phase Test Facility (TPTF) of the Japan Atomic Energy Research Institute (JAERI) are used to study the issues related to the calculation of dry out and post-dry out in rod bundle using a one-dimensional, two-fluid, three-field model. Details of the model are discussed in Section 2 while the results are presented in Section 3.

2. Details of the one-dimensional three-fluid model

2.1. Governing equations

The present three-fluid calculation scheme is based on an extension of the two-fluid model of the CATHARE code [7]. Three sets of one-dimensional mass, momentum and energy conservation equations are solved for the three fluids, namely, gas or vapour (v), continuous liquid flowing in the form of a film (lc) and dispersed liquid flowing in the form of entrained droplets (ld). This allows for different liquid velocities and temperatures for the two liquid fields. No restrictive hypothesis has been made about the droplet temperature, which is obtained from its own energy balance equation. Thus, the model features nine independent balance equations. The corresponding main variables are the three phasic velocities V_v, V_{lc}, V_{ld}, the three phasic enthalpies H_v, H_{lc}, H_{ld}, one common pressure P and two volume fractions α_v, α_{ld} for gas and liquid droplets. The set of conservation equations is listed in Appendix A.

The physical significance of many of the terms appearing in the above equations is well-known (see for example [29]). Terms that are specific to the current model are discussed briefly here. In the mass balance terms, inter-phase terms, Γ_k, expressed here in terms of rate of mass transfer per unit volume, appear. The terms Γ_{lcv} and Γ_{ldv} represent mass transfer with phase change due to boiling and condensation, respectively, and are, respectively, positive and negative source terms for the vapour phase. The terms Γ_a and Γ_d represent mass transfer without phase change between the continuous liquid field and the droplet field, and are associated, respectively, with the processes of droplet entrainment from and the redeposition to the continuous liquid phase. These constitute, respectively, negative and positive source terms to the continuous liquid field. The momentum balance equations have been expressed in non-conservative form so that the phasic velocity, V_k, appears as the principal variable. The terms involving p_{ik} in the momentum equations are related to the interfacial pressure and are needed to maintain hyperbolicity of the system of equations. The term involving β is the added mass term; terms involving τ_i are inter-phase shear stresses; those involving χ_f, the wetted perimeter, are wall shear stresses; and those involving the parameter R account for stratification effects in horizontal flow [7] and are set to zero in the present case dealing with vertical annular flow. Finally, in the phasic energy balance equations, distinction is made between inter-phase heat transfer, q_{ik}, expressed per unit volume, and phase-wall heat transfer, q_{wk}, expressed per unit surface area. The heated perimeter, χ_h, is used to convert the latter into a volumetric source term. In addition, wall–liquid interface heat transfer terms, q_{wic} and q_{wid}, expressed per unit interfacial area, are used to enable thermal non-equilibrium of the liquid phase in the general case. The parameters, $\chi_{h,c}$ and $\chi_{h,d}$ are used to convert these into volumetric sources.

The above set of nine conservation equations differs from the set of seven used by Hoyer [14] but is similar to that used by Sugawara [30]. The constitutive laws for the various terms in the equations are, however, different, as will be seen below. The present formulation allows for the solution of the velocities directly while that of Sugawara solves for momentum as the solution variable.

2.2. Closure relations

A number of closure relations are required to evaluate many of the right hand side terms in the above set of equations. These represent interphase exchange, wall-phase exchange, etc. These are discussed in detail in Jayanti and Valette [17] and the principal ones are summarized here:

- The droplet entrainment flux, Γ_a, is modelled as a sum of the contributions from two processes, namely, entrainment arising from the shearing action of gas flowing over a wavy surface, Γ_{ah}, and creation of droplets in the process of nucleate boiling due to break-up of bubbles, Γ_{ab}. The first of these components, Γ_{ah}, is evaluated using the empirical correlation of Hewitt and Govan [12] while the second component is calculated using the correlation proposed by Ueda et al. [31].
- The droplet deposition flux, Γ_d, is evaluated based on the turbulent diffusion model of Hewitt and Govan [12]. An additional term, based on Hoyer [14], is used

to account for the inhibition of droplet deposition by the steam flux caused by evaporation. Thus, the net deposition flux per unit volume, Γ_d, is evaluated as

$$\Gamma_d = \frac{4}{D_h}\rho_{ld}\frac{\alpha_{ld}}{\alpha_{ld}+\alpha_v}\max(k_d - k_q, 0) \quad (1)$$

where k_d is the deposition coefficient given by Hewitt and Govan [12] and k_q is the deposition inhibition coefficient due to evaporation:

$$k_q = \frac{\Gamma_{lcv} D_h}{0.26\rho_{lc}}\frac{1}{\sqrt{\alpha_{ld}+\alpha_v}} \quad (2)$$

In the momentum balance equations, any momentum exchange resulting from friction between the wall and the dispersed phase due to bouncing, etc., is neglected. For the other two phases, the coefficient C_k appearing in the respective momentum equations is evaluated as

$$C_k = \mathrm{Max}\left\{\frac{16}{Re_k}, \frac{0.079}{Re_k^{0.25}}, 0.005\right\} \quad \text{with}$$

$$Re_k = \frac{\alpha_k\rho_k \mid V_k \mid D_h}{\mu_k} \quad (3)$$

If the wall is wetted by a liquid film, then the wall–gas momentum exchange is zero.

- The friction-related interfacial momentum exchange involves three terms: the liquid droplet–liquid film exchange, the liquid droplet–gas exchange and the liquid film–gas exchange. The first one is neglected while the second one is dealt with using a classical formulation of droplet drag in a gas flow with a constant drag coefficient, C_d, of 0.5. The interfacial friction between the continuous liquid phase and the gasphase is strongly flow regime-dependent. For annular flow conditions, a purely geometric relation, based on the single phase flow through fully-rough pipes (thus there being no influence of gas phase Reynolds number on the friction factor) is used to evaluate the interfacial friction factor:

$$f_i = \frac{0.331}{\left[\ln\left(\frac{k_s}{3.71D_h}\right)\right]^2} \quad \text{where } \frac{k_s}{D_h} = 2.25\alpha_{lc}^{1.7} \quad (4)$$

The interfacial shear stress between the gas and the liquid film is evaluated as

$$\tau_{icv} = \frac{4}{D_h}\left(1-\frac{\alpha_{lc}}{2}\right)f_i\rho_v \mid V_v - V_{lc} \mid (V_v - V_{lc}) \quad (5)$$

- In the energy balance equations, various heat flux terms appear. These can be grouped under two categories: heat transfer involving the wall and interfacial heat transfers. It is assumed that the liquid droplets are not directly heated or cooled by the wall. Thus, q_{wld} (transfer from wall to liquid droplets) and q_{wid} (transfer from wall to liquid droplet interface) are set to zero. The heat transfer from the wall to the continuous liquid or the gas phase is modelled as being due to forced convection. Two cases are distinguished for the heat transfer from wall to continuous liquid interface, q_{wic}. When $T_w \geqslant T_{sat}(P)$, a nucleate boiling mode is assumed and the Thom correlation [1] is used to calculate the heat flux. When $T_w \leqslant T_{lc} \leqslant T_{sat}(P)$, heat transfer is assumed to occur by film condensation. An approximate value of 2000 W/m^2 K for film condensation heat transfer coefficient is used to calculate the heat flux. In all the other cases, q_{wic} is set to zero. The heat flux from the gas to the interface of the dispersed liquid is evaluated using a convection law for flow around spheres [32] and that from the gas to the interface of continuous liquid is modelled using a forced convection approach. Finally, the heat flux from the dispersed liquid to its interface (q_{ldi}) and that from the continuous liquid to its interface (q_{lci}) are evaluated using a flashing or condensation formulation depending on whether the phasic temperature T_k is greater or less than the saturation temperature.
- The onset of annular flow is determined based on a limiting Kutateladze number and minimum quality as

$$Ku_v > 3.2 \text{ and } x > 0.1 \quad \text{where}$$

$$Ku_v = V_v\left(\frac{\rho_v^2}{[g\sigma(\rho_{ld}-\rho_v)]}\right)^{\frac{1}{4}} \quad (6)$$

The limit of $x > 0.1$ may delay the onset of annular flow at low pressures; however, this would not affect the predictions of dry out and post-dry out heat transfer as dry out rarely occurs at such low qualities at low pressures. The minimum quality condition is essential for the prediction of dry out at high pressures [17].

- Finally, the droplet diameter is an important parameter in determining the post-dry out heat transfer and is evaluated using the following expression:

$$\frac{\delta}{\ell} = (2.5We^{-0.58} + 0.1\alpha_{ld}^{0.25}) \quad (7)$$

Here ℓ is the Laplace length and the Weber number is defined based on the Laplace length:

$$\ell = \sqrt{\sigma/g\Delta\rho} \quad We = \rho_v V_v^2 \ell/\sigma \quad (8)$$

The set of equations listed in Appendix A along with the above closure relations have been used to calculate for several cases [33] of dry out in a single tube. The predicted dry out quality is compared with the experimental value in Fig. 2 in the pressure range of 30–200 bar and in the mass flux range of 500–3000 kg/m^2 s. It is seen that good agreement is obtained over this wide range of parameters.

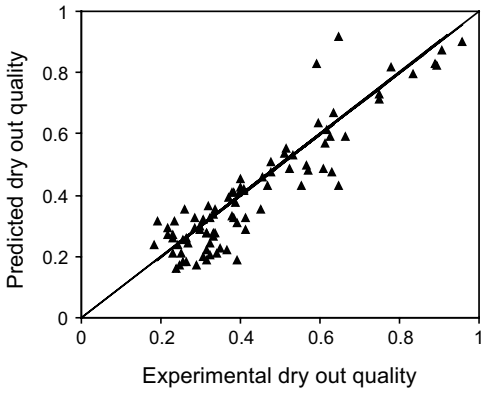

Fig. 2. Comparison of the predicted dry out quality with that measured by Becker et al. [33] for flow inside a tube over a pressure range of 30–200 bar, a mass flux range of 500–3000 kg/m^2 s and a tube inner diameter range of 10–24.7 mm.

2.3. Modelling of rod bundle

The approach used in the present study towards dealing with a rod bundle is to use the same set of conservation and closure equations as for flow inside a tube. The justification for this arises from a consideration of the factors involved:

- The Reynolds numbers based on hydraulic diameter and phasic properties are usually very high and it is therefore expected that a simple hydraulic diameter approach to flow through non-circular cross-section, i.e., only replacing the tube diameter by the bundle or the sub-channel hydraulic diameter in the Reynolds number calculation, would be fairly accurate.
- Available evidence (Wurtz, [21]) from flow through annular geometries suggests that the entrainment process for a film outside the tube is not very different from that inside the tube for thin films. Hence the dynamics of the entrainment processes occurring in the rod bundles is expected to be represented well by in-tube flow correlations.
- The deposition of droplets is assumed to be governed by turbulent diffusion effects and it is expected that, provided the correct tube surface area is considered (using the wetted perimeter approach), the same set of correlations can also be used.
- Making use of the heated perimeter approach, the correct heat transfer area can be included in the calculation. From the energy balance, this would produce the correct equilibrium quality variation within the rod bundle. Also, the nature of annular flow is expected to be similar for flow outside the tubes and inside the tubes as the film thickness is small and other factors are turbulence-driven. Thus, similarity of local conditions can be ensured by maintaining correct energy balance and correct rates of entrainment and redeposition, which depend on the local phasic velocities etc., can be calculated.

The geometric details of a rod bundle are different from those of a single tube and there may be three-dimensional effects. These obviously cannot be taken into account implicitly in a one-dimensional calculation procedure and the only geometric parameters that are relevant here are the volume, the flow cross-sectional area and the wetted and heated perimeters in each cell of a one-dimensional representation of a rod bundle. There are several ways of reckoning these parameters; the two most common being a sub-channel approach and a whole-channel approach. In the sub-channel approach, presence of outside walls is neglected and the flow cross-sectional area and the hydraulic diameters are calculated on a "unit cell" which is well-inside the bundle. The whole-channel approach considers all the tubes and all the walls in the calculation of these geometric parameters. For a large tube bundle, the two approaches should give nearly the same values; however, considerably different results may be obtained for when the number of tubes in the rod bundle is small. In the present study, two test series were considered. These are the TPTF test series of JAERI on a 5×5 rod bundle and the THTF test series of ORNL on an 8×8 rod bundle. The effect of whole-channel and sub-channel approaches was investigated as part of the present study for the TPTF test series while only the sub-channel approach was used for the THTF test series.

Another geometrical feature that is present in rod bundles only is the spacer grid which is used to support the rod bundles. The effect of spacer grids on the dry out is usually modelled by modifying empirically the entrainment and deposition rate processes [26,13]. In the present study, the closure relations are kept unchanged and the geometric parameters, namely, the flow cross-sectional area and the hydraulic diameters are changed locally (i.e., in the cells containing the spacers grids) taking into effect the geometric details of the spacer grids. Accordingly, in the THTF test series, the flow cross-sectional area in the spacer grid cells is reduced by about 12% and the hydraulic diameter by a factor three. As will be shown later, fairly good agreement with the data is obtained with this modelling. In the TPTF test series, the available temperature data are well-away from the spacers and no effect of spacers could be seen. Also, in these data, dry out occurred at a very high quality and in such cases, as will be shown later, the effect of spacers is highly localized and there is virtually no effect of the spacer grids on the post-dry out temperature variation. Also, details of the spacer grids are not available. In view of these factors, the

TPTF test series calculations were done without considering spacer grid effects.

2.4. Numerical details

The numerical calculation scheme is similar to that employed in the CATHARE code [34]. The set of conservation equations and closure relations is discretized using a finite difference scheme with staggered spatial mesh and the donor-cell method. A fully implicit scheme is used to deal with the temporal derivatives in which the terms dealing with interphase exchange, pressure propagation and convection are evaluated implicitly. This removes any Courant number limitation on the time step. The solution of the discretized non-linear equations is carried out using the Newton-Raphson iterative method in which the Jacobian is re-evaluated at each iteration. Analytical derivatives for each equation and each closure relation are used systematically to evaluate the Jacobian. While there is no Courant number limitation on the time step, the non-linearity of the equations may cause convergence difficulties in case of large transients or at points of discontinuity in the constitutive models. An automatic time step management scheme is used to adjust the time step dynamically.

Although only steady state solution is required in all the cases considered here, the calculations were carried out in a transient mode. The heat flux is linearly increased from zero to the final steady state value imposed in the experiments and all the boundary conditions are kept constant from that point onwards. The flow conditions and wall temperatures reach steady values, typically, in several tens of seconds. The number of nodes used to discretize the rod bundle depended on the case. In the TPTF test series, where the inlet quality was typically of the order of 0.7 and where the spacer grids were not considered, 30 nodes were used. In the THTF test series, where the inlet was sub-cooled liquid and where the effect of the spacer grids was sought to be resolved, a total of 90 nodes were used. Typically, one calculation with 30 nodes for 200 s of time took one to two minutes on a single CPU of the HP 9000/800 computer.

3. Results

3.1. Details of the test cases

Two sets of data in which wall temperature measurements were carried out systematically in rod bundles are used in the present study to validate the current calculation procedure. The first of these was obtained at the Two-Phase Test Facility (TPTF) of the Japan Atomic Energy Research Institute (JAERI) [28] in a 5×5 rod bundle consisting of rods of 12.27 mm outer diameter and a heated length of 3.7 m arranged in a square pitch of 16.16 mm. Outside wall temperature measurements were carried out at 11 axial locations on 9 out of the 25 heated rods. All the tests (about 25 individual test series with heat flux being varied within each series) were conducted under a mixed inlet condition, i.e., a condition where steam and water mixture enters the test section. The test conditions covered the pressure range of 30–120 bar, mass flux range of 20–410 kg/m^2 s and inlet quality range of 0.4–0.9. Specific series of experiments were conducted to investigate the effect of inlet quality at fixed mass flux at high and low pressures; the effect of mass flux at fixed inlet quality and pressure; and the effect of pressure at fixed inlet quality and mass flux. Considerable scatter in the dry out location was observed, and although the wall heat flux was uniform along and across the bundle, dry out was found to occur earlier for peripheral rods than for central rods. Typical results for one particular case (run #115) are shown in Fig. 3 at a system pressure of 30 bar and mass flux of 300 kg/m^2 s. Considerable variation in the wall temperature within the bundle can be seen. The five central rods in Fig. 3a show considerable variation of the location of the dry out point as well as in the post-dry out evolution of the wall temperature. The data of rod #8 (plotted as a

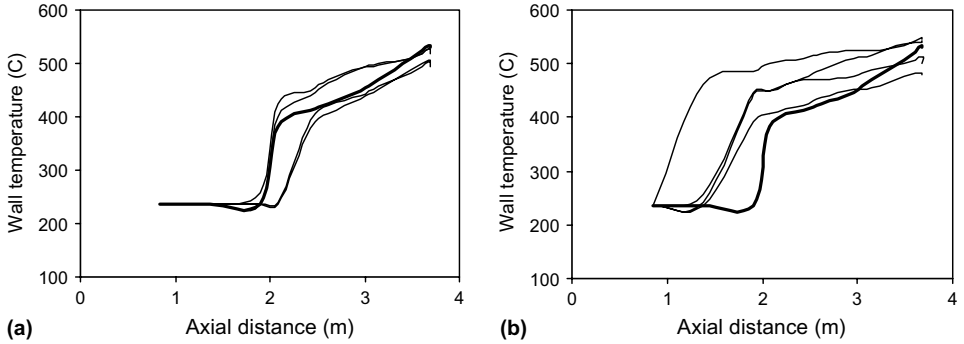

Fig. 3. Measured wall temperature variation for (a) five central rods and (b) four peripheral rods in the 5×5 rod bundle for test #115 in the TPTF test series. The thick line corresponds to rod #8, the wall temperatures of which are available for comparison.

thick line) were taken by Kumamaru et al. [27] as being representative of the wall temperature variation. The four peripheral rods in Fig. 3b show an earlier dry out (compared with that of the thick line corresponding to the central rod #8) and also considerable scatter in the wall temperature variation.

The second set of data were obtained at the Thermal Hydraulic Test Facility (THTF) of ORNL, Tennessee, USA [27] in a 8×8 rod bundle with a geometry typical of 17×17 PWR cores. The rods, of a length of 3.66 m, had a diameter of 9.55 mm and were placed on a 12.7 mm pitch. Sixty of the 64 rods were electrically heated with axially and radially uniform profiles. Egg-crate type spacer grids without swirl inducers were used at 0.6 m intervals to support the bundle. The rod temperatures were measured at 25 axial locations with detailed thermometry above and below each of the two topmost spacer grids to bring out the effect of the spacer grids on the heat transfer. The test parameters covered a wide range of parameters typical of a postulated nuclear reactor loss-of-coolant accident (LOCA) condition with pressure in the range of 44–134 bar, mass flux in the range of 43–815 kg/m^2 s and equilibrium quality in the range of 0.4–1.3. The test section inlet was always under sub-cooled liquid condition; hence the heat fluxes were considerably higher than those used in the TPTF test series for similar system pressure and mass flux. As expected, rod-to-rod variation was found in the wall temperatures at a given axial location and dry out of the bundle stretched over a short length of the bundle. Yoder et al. reported the *average* wall temperature of all *dry* rods (defined as having a superheat of 222 K) in case some of the rods were wet. In all 30 individual cases were reported from which 18 distinct cases (with one of the three parameters—pressure, mass flux or heat flux—varying by 10% or more) can be constructed.

3.2. Comparison with the TPTF test series

Calculations for 28 cases of the TPTF test series were made covering the range of parameters reported by Kumamaru et al. [28]. The predicted locations of dry out for the ensemble of these test cases is compared with the experimental value in Fig. 4. Here, the predictions are based on sub-channel model as well as on a whole-channel model of the bundle are given. (It should be noted that because of the different flow cross-sectional areas, the mass flux is different for sub-channel and whole-channel modelling of the rod bundle. If this is not adjusted appropriately, a wrong prediction of the dry out location results.) The whole-channel model predicts a slightly later dry out than the sub-channel model. The experimental value is based on the wall temperature variation of rod #8 alone. As shown in Fig. 3, there can be considerable variation from rod-to-rod, and additional

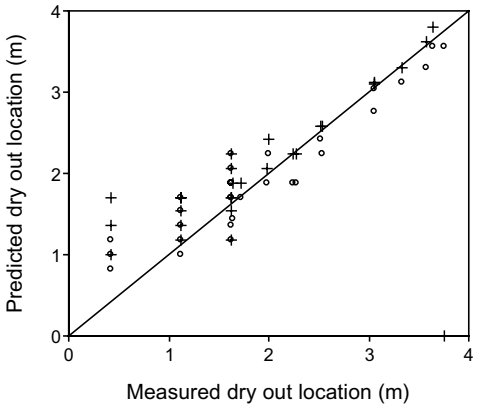

Fig. 4. Comparison of the predicted and the experimental dry out distance for a number of cases in the TPTF test series. The predictions made using a sub-channel model (circles) and a whole-channel model (plus) are shown.

uncertainty arises for the low dry out length cases because of lack of instrumentation. In view of all these, the agreement between the predictions and the data can be considered to be good. This is not surprising because in nearly all cases, dry out occurs for quality greater than 0.9 due to the combination of low mass flux and low heat flux leading to low entrainment of the liquid film. Thus, in some cases, the prediction of dry out location reduces to one of determination of equilibrium quality variation.

The effect of individual parameters is shown in Figs. 5–8. The effect of varying system pressure in the range of 118–31 bar at nearly constant mass flux and inlet quality is shown in Fig. 5. The effect of varying mass flux between 777 and 116 kg/m^2 s at a system pressure of 118 bar and at nearly constant inlet quality of 0.76 is shown in Fig. 6. The effect of varying the heat flux in the range of 110–720 kW/m^2 at a system pressure of 31 bar, mass flux of 310 kg/m^2 s and inlet quality of 0.76 is shown in Fig. 7. Finally, the effect of varying the inlet quality in the range of 0.89–0.19 at a system pressure of 118 bar and at nearly constant mass flux is shown in Fig. 8. In all the cases, the predicted wall temperature variation is compared with that of the rod #8 measured experimentally. Although there is deviation in terms of both location of dry out and subsequent variation of the wall temperature, it is probably within the experimental variation within the bundle (see Fig. 3 above). It can be said that the post-dry out heat transfer is captured fairly well by the model.

3.3. Comparison with the THTF test series

The THTF test series is characterized by high heat fluxes when compared to the TPTF test series. The pres-

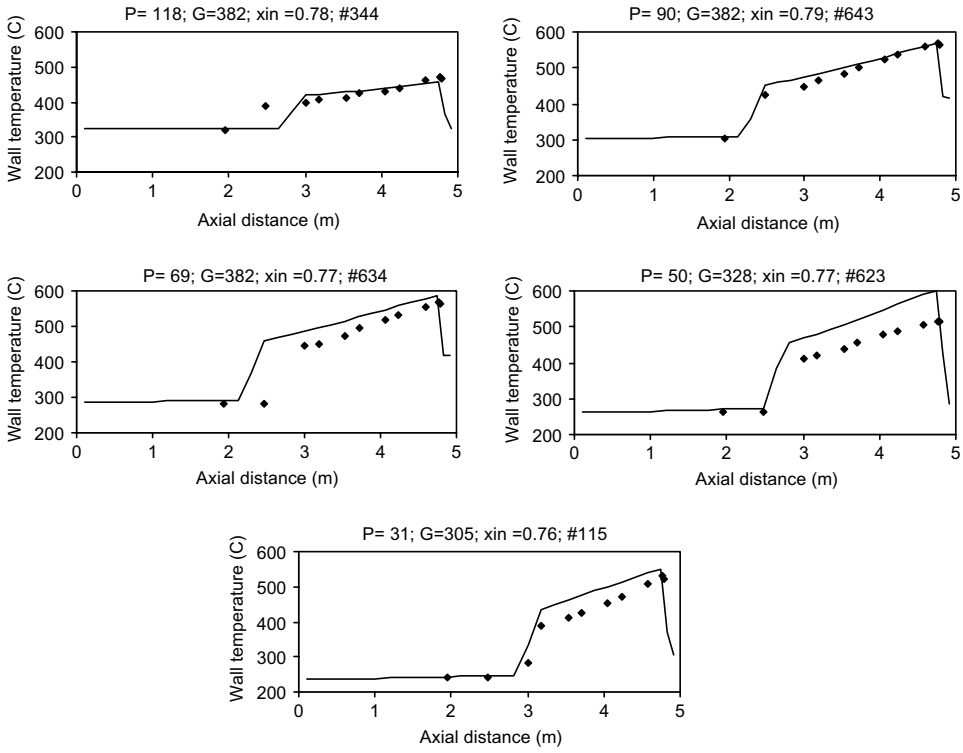

Fig. 5. Effect of pressure on wall temperature variation: comparison between predictions and the data on rod #8 from TPTF test series. The pressure (in bar), mass flux (in kg/m^2 s), inlet quality and the case number are indicated in each figure.

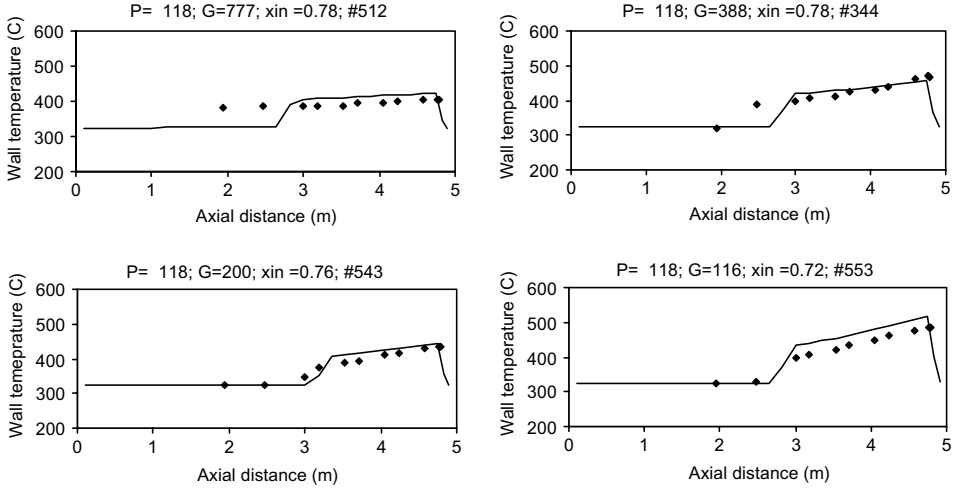

Fig. 6. Effect of mass flux on wall temperature variation: comparison between predictions and the data on rod #8 from TPTF test series. The pressure (in bar), mass flux (in kg/m^2 s), inlet quality and the case number are indicated in each figure.

sure ranges from 40 to 135 bar and the mass flux from 250 to 800 kg/m^2 s. In addition to these, six low flow tests have been conducted, four of which are at around 80 bar and the other two at around 40 bar, in which the mass flux ranges from 43 to 172 kg/m^2 s. Calculations show that in these tests, there is negligible entrainment and the dry out occurs at qualities greater than 0.95. Indeed, the mass flux is so low that in some cases, the three-field model reduces to a two-field model as the droplet concentration is zero. However, in cases where

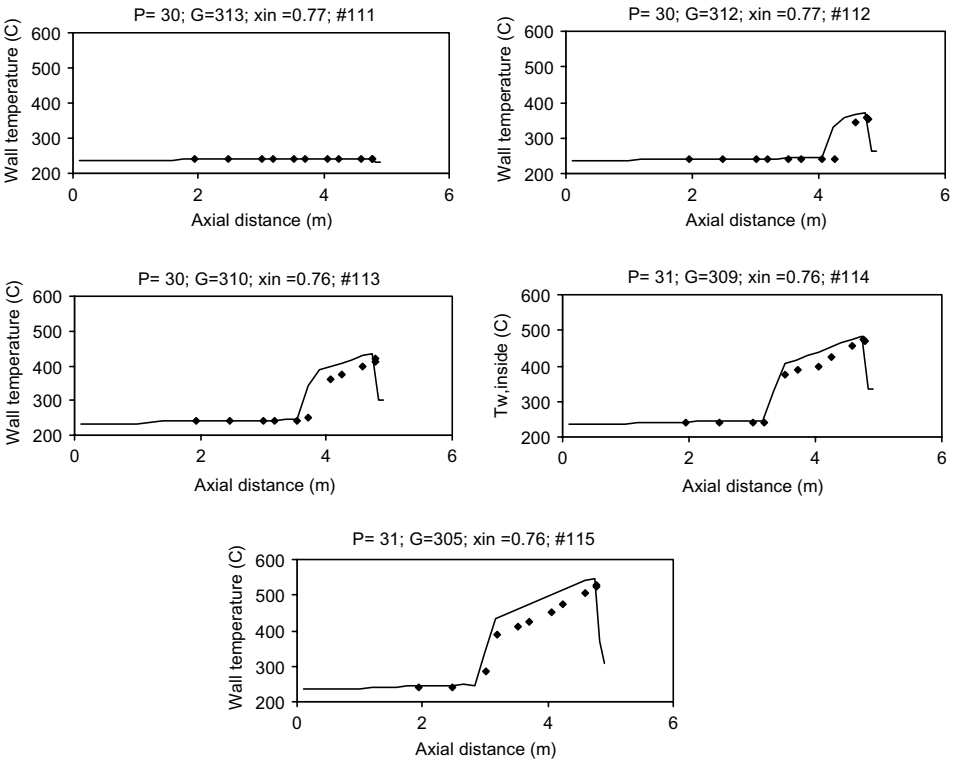

Fig. 7. Effect of heat flux on wall temperature variation: comparison between predictions and the data on rod #8 from TPTF test series. The pressure (in bar), mass flux (in kg/m^2 s), inlet quality and the case number are indicated in each figure.

the mass flux is greater than about 200 kg/m^2 s, significant entrained droplet flux exists and dry out occurs at qualities as low as 0.39 (for Case B). As in the case of the TPTF series, significant rod-to-rod variation exists within the bundle, and for a given case a section of the bundle may be under partial dry out condition in which some of the tubes are wet and the rest dry (defined by Yoder et al. [27] to have a superheat in excess of 222 °C). An experimental value of the dry out quality can be therefore estimated by reckoning dry out to have occurred at that point at which a majority of the tubes are dry. This estimated dry out quality is compared in Fig. 9 with the predicted value obtained from the calculation methodology outlined in Section 2. It can be seen that except for a couple of cases, the predicted quality agrees well with the experimental value. As remarked previously by Hoyer [14] and Jayanti and Valette [17], at high pressures, heat flux has a significant effect on the droplet flux. The comparison in Fig. 9 shows that this is captured well by the combination of terms representing nucleate boiling-induced entrainment (given by correlation of Ueda et al., [31]) and evaporation flux-induced suppression of droplet deposition (given by equation (2) above).

Another distinguishing feature of the THTF test series is the effect of spacers on the post-dry out heat transfer. In the present study, the effect of spacer grids has been included by incorporating their geometric details in the calculation procedures in the cells in which they are located. In order to bring out their effect explicitly, calculations have been done without taking account of the spacer grid details. Comparison of the results obtained with the two treatments shows that the possible effect of spacer grids on dry out varies from case to case. This is brought out in Fig. 10 where the axial variation of the fraction of the droplet mass flux (i.e., the droplet mass flux divided by the total mass flux) is compared with the two treatments of the spacer for three different cases, namely, Cases B, D and F, all of which are at a system pressure of 127 bar. The corresponding mass fluxes are 713, 517 and 255 kg/m^2 s, respectively. In each case, the corresponding dry out location is indicated on the abscissa. In the initial part of the tube where sub-annular flow regimes occur, the droplet mass fraction is zero; it then increases to a maximum value before decreasing. The figures reveal the interesting effect of spacer grids. Due to the decreased hydraulic diameter at the spacer, the droplet deposition rate locally increases; this reduces the droplet mass fraction. Subsequently, this is re-entrained in the usual way. The rapidity with this is re-entrained and the overall droplet fraction together contribute to the net effect of spacer

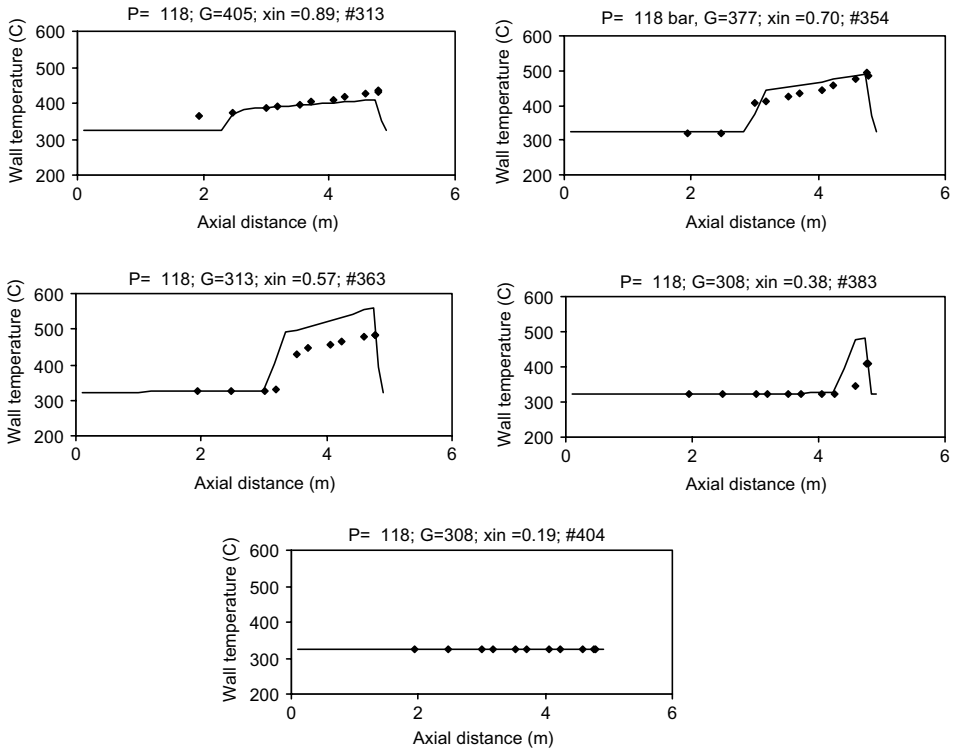

Fig. 8. Effect of inlet quality on wall temperature variation: comparison between predictions and the data on rod #8 from TPTF test series. The pressure (in bar), mass flux (in kg/m^2 s), inlet quality and the case number are indicated in each figure.

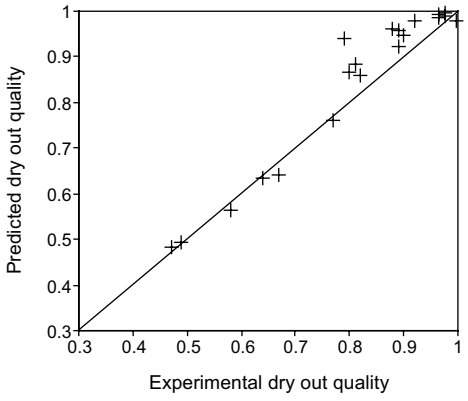

Fig. 9. Comparison between the predicted and the estimated dry out qualities for a number cases of the THTF test series.

grids on the dry out. In Fig. 10a, the mass flux is high and hence the entrainment rate is also high; thus there is quick recovery of the deposited droplets at the spacers resulting in little change in the overall droplet mass fraction around the spacers. In Fig. 10b, the mass flux is lower and there is only a gradual recovery of the droplet fraction following forced deposition at a spacer grid. Since spacer grids are periodically placed, there is a cumulative effect because of which the entrained fraction curve is significantly lower than the case where the spacer grid effect is neglected. This results in a substantial change in the dry out location. In Fig. 10c, the mass flux is even lower leading to even slower recovery following forced deposition at a spacer grid. However, the entrained fraction itself is significantly lower due to low overall entrainment and the net effect on dry out is nearly negligible.

The effect of system pressure is investigated in Fig. 11 where similar plots for Cases J, M and P are compared at system pressures of 134, 86 and 60 bar, respectively. The corresponding mass fluxes are 731, 656 and 520 kg/m^2 s, respectively. As the system pressure increases, the vapour density increases and the entrained fraction is higher. The net entrainment rate is higher. As a result, the entrained fraction curve with the spacer grid effects included deviates little from the one where spacer grid effects are neglected at high pressures (Fig. 11a) resulting in little net effect on the location of dry out. In Fig. 11b, the pressure is lower and the entrained fraction and the net entrainment rate are lower. The combination of these gives rise to a very significant effect of the spacer grids on the dry out location. In Fig. 11c, the significantly lower entrained fraction at the lower

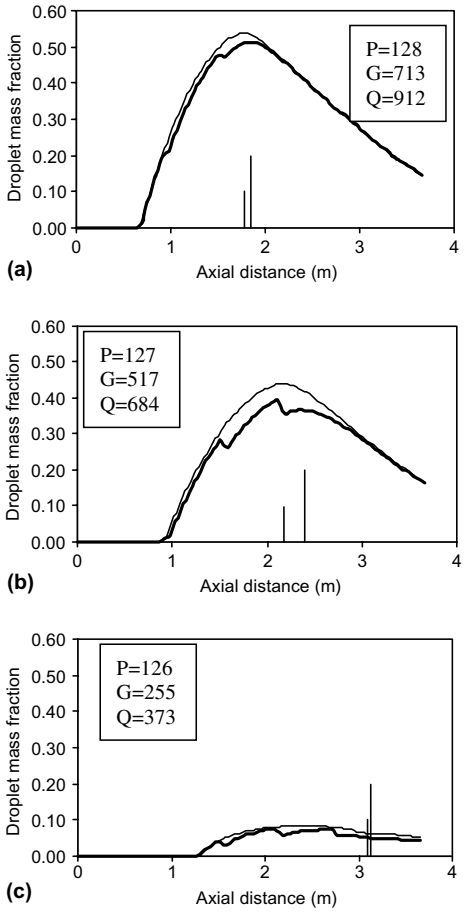

Fig. 10. Calculated variation of the entrained mass fraction with axial distance with (thick line) and without (thin line) including the spacer grid geometric details for Cases B, D and F of the THTF test series. The long and short vertical lines on the abscissa in each figure indicate the calculated dry out locations with and without the spacer details, respectively. The pressure P (in bar), mass flux G (in kg/m^2 s) and heat flux Q (in kW/m^2) are indicated in each figure.

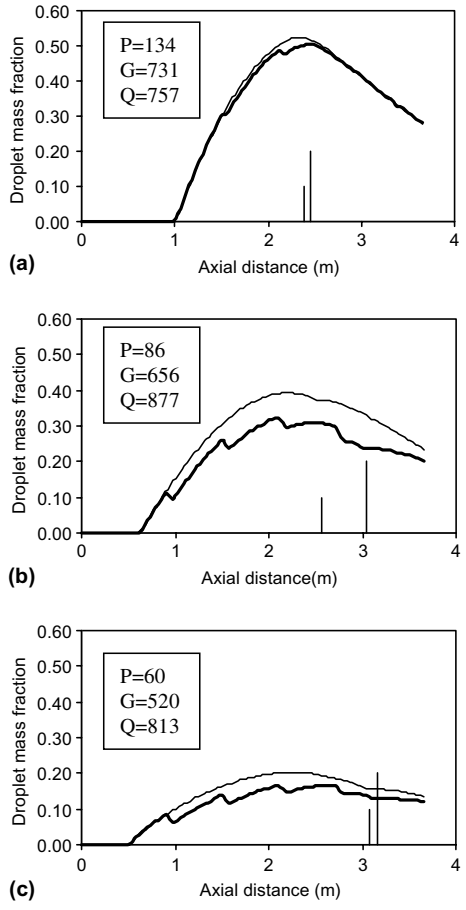

Fig. 11. Calculated variation of the entrained mass fraction with axial distance with (thick line) and without (thin line) including the spacer grid geometric details for Cases J, M, P of the THTF test series. The long and short vertical lines on the abscissa in each figure indicate the calculated dry out locations with and without the spacer details, respectively. The pressure P (in bar), mass flux G (in kg/m^2 s) and heat flux Q (in kW/m^2) are indicated in each figure.

pressure results in a somewhat muted effect of the spacer grid on the dry out location. Thus, the specific effect of spacer grids on the location of dry out depends on a number of factors related to the entrainment and redeposition processes.

Finally, the effect of the spacer grids on the post-dry out heat transfer is brought out in Fig. 12 where the predicted wall temperature variation with and without spacer grids is compared with the measured data for several cases. These include:

- Cases B, D and C in Fig. 12a at a system pressure of 127 bar and mass fluxes of 713, 517 and 334 kg/m^2 s, respectively. Here, the wall temperature variation in the post-dry out region shows a decreasing, nearly flat and increasing tendency with distance from the dry out location. This is due to the contribution of droplets to post-dry out heat transfer and has been observed in flow through single tubes [17]. At low mass fluxes (Case C), the dry out quality is so high that there is very little contribution of droplets to heat transfer because of which the wall temperature continues to rise (Fig. 12a(iii)) whereas the presence of large amount of droplets in Case B actually reduces the post-dry out wall temperature (Fig. 12a(i)). These effects are well-captured in the model. The presence of spacers affects only the local temperature variation around the spacers due to the dominant contribution of the droplets to the heat transfer.

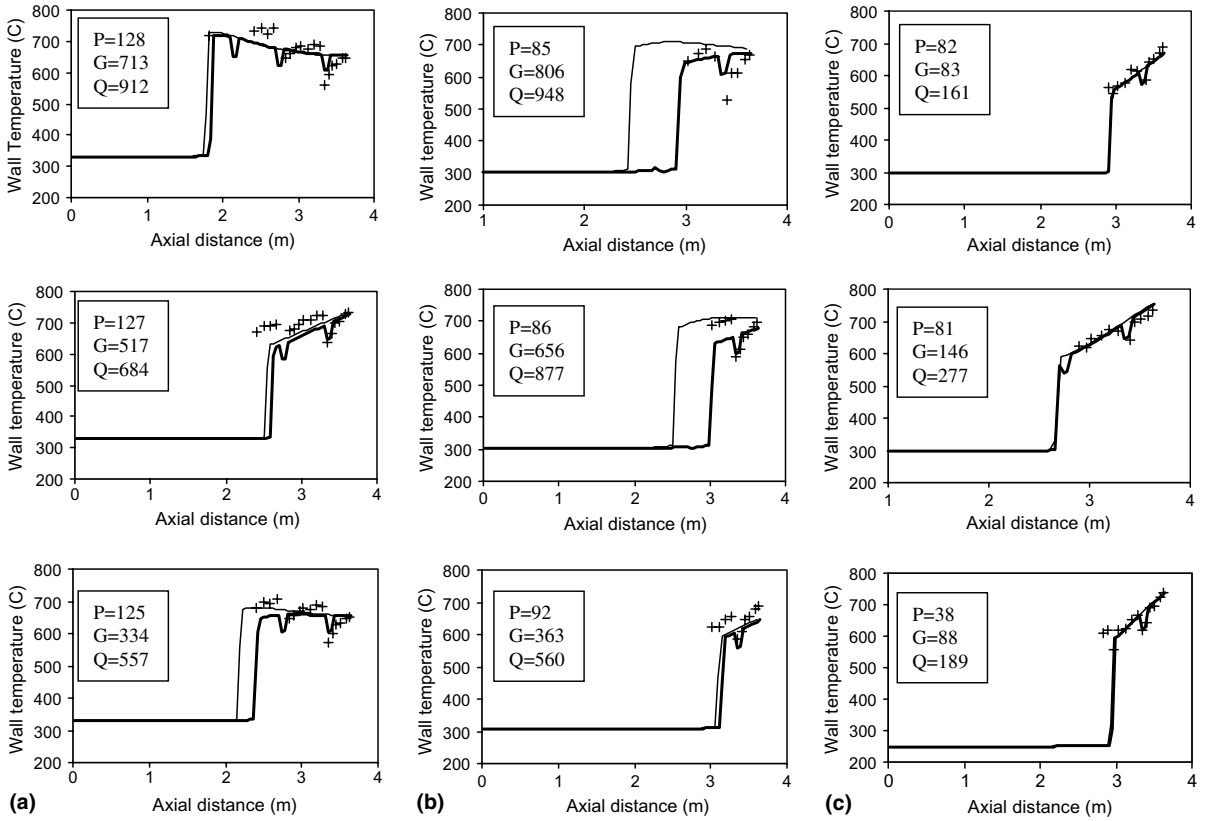

Fig. 12. Comparison of the measured and the predicted axial variation of the wall temperature for three cases illustrating (a) effect of mass flux at a pressure of around 130 bar; (b) effect of mass flux at a pressure of 85 bar; and (c) variation at very low mass fluxes. The calculated variation with (thick line) and without (thin line) including the spacer grid geometric details are shown. The pressure P (in bar), mass flux G (in kg/m^2 s) and heat flux Q (in kW/m^2) are indicated in each figure.

- Cases N, M and I at a system pressure of about 86 bar for mass fluxes of 806, 656 and 363 kg/m^2 s, respectively. Here, the effects are similar to those in Fig. 12a. The temperature rise following dry out is higher at this pressure compared to that at 125 bar, and the effect of spacers on the wall temperature variation persists in some cases (Fig. 12b(ii)). Hence the beneficial effect of spacers on dry out quality translates into reduced wall temperature in such cases.
- Cases IB, ID and IE under low flow conditions at system pressures of 82, 81 and 38 bar, respectively, and at mass fluxes of 83, 146 and 88 kg/m^2 s, respectively. Here, the mass fluxes are so low that dry out occurs at qualities of near unity and there is very little influence of droplets on post-dry out heat transfer. The spacer grids also have very little influence on dry out location, as noted above, and their effect on the wall temperature variation in the post-dry out region is purely convective and purely local. It is noted that taking account of geometrical effects such as reduced flow cross-section and hydraulic diameter enables the correct prediction of the temperature decrease at the spacer grids in these cases.

It can be seen from the plots in Fig. 12 that in general fairly good agreement is obtained for the prediction of dry out location as well as for the wall temperature variation in the post-dry out region within the tube bundle over the range of parameters investigated.

4. Conclusions

A new three field model is developed in order to simulate two phase flow and heat transfer in nuclear reactor accident conditions. The liquid phase is split up into liquid droplets and continuous liquid. A number of issues related to the calculation of dry out and post-dry out heat transfer in rod bundles have been studied. It is shown that good agreement with data can be obtained for the prediction of the location of dry out and of the further evolution of the rod wall temperature variation using:

- The same set of constitutive equations for mass, momentum and energy exchanges as for flow inside tubes.
- A sub-channel model for the calculation of geometrical parameters of the rod bundle that enter into the calculation procedure (instead of a whole subassembly model).
- Taking account of spacer grids by treating each spacer grid section as a separate cell and modifying only the geometrical parameters in these cells.

This approach has been shown to give fairly accurate representation of dry out and post-dry out heat transfer in typical BWR and PWR type rod bundles in the pressure range of 30–135 bar, mass flux range of 50–800 kg/m^2 s over a range of heat fluxes and inlet conditions. The essential features of the flow and heat transfer characteristics in the rod bundle appear to have been captured well in the parametric range studied.

Acknowledgments

This work was made in the frame of the development of the NEPTUNE code, which is jointly developed by the Commissariat à l'Energie Atomique (CEA, France) and Electricité de France (EDF) and also supported by the Institut de Radioprotection et de Sûreté Nucléaire (IRSN, France) and FRAMATOME-ANP. The authors are grateful to JAERI for making available the TPTF data and to ORNL for the THTF data.

Appendix A. Set of balance equations

Mass balance of gas field

$$\frac{\partial}{\partial t}(A\alpha_g\rho_g)+\frac{\partial}{\partial z}(A\alpha_g\rho_g V_g)=+A(\Gamma_{lcv}+\Gamma_{ldv})$$

Mass balance of continuous liquid field

$$\frac{\partial}{\partial t}(A\alpha_{lc}\rho_{lc})+\frac{\partial}{\partial z}(A\alpha_{lc}\rho_{lc}V_{lc})=+A(\Gamma_d-\Gamma_a-\Gamma_{lcv})$$

Mass balance of dispersed liquid field

$$\frac{\partial}{\partial t}(A\alpha_{ld}\rho_{ld})+\frac{\partial}{\partial z}(A\alpha_{ld}\rho_{ld}V_{ld})=-A(\Gamma_d-\Gamma_a+\Gamma_{ldv})$$

Momentum balance of gas field

$$\begin{aligned}&A\alpha_g\rho_g\left[\frac{\partial V_g}{\partial t}+V_g\frac{\partial V_g}{\partial z}\right]+A\alpha_g\frac{\partial P}{\partial z}-Ap_{ilcg}\frac{\partial\alpha_{lc}}{\partial z}-Ap_{ildg}\frac{\partial\alpha_{ld}}{\partial z}\\&+A\beta\alpha_g\alpha_{lc}\rho_m\left[\frac{\partial V_g}{\partial t}-\frac{\partial V_{lc}}{\partial t}+V_g\frac{\partial V_g}{\partial z}-V_{lc}\frac{\partial V_{lc}}{\partial z}\right]\\&=A\Gamma_{lcv}(W_{icv}-V_g)+A\Gamma_{ldv}(W_{idv}-V_g)-A(\tau_{icv}+\tau_{idv})\\&-\chi_f C_g\frac{\rho_g}{2}V_g\mid V_g\mid+A\alpha_g\rho_g g_z+\frac{R\alpha_{lc}}{4}p_{ilcg}\frac{\partial A}{\partial z}\\&\text{with }\rho_m=\alpha_g\rho_g+\alpha_{lc}\rho_{lc}\end{aligned}$$

Momentum balance of continuous liquid field

$$\begin{aligned}&A\alpha_{lc}\rho_{lc}\left[\frac{\partial V_{lc}}{\partial t}+V_{lc}\frac{\partial V_{lc}}{\partial z}\right]+A\alpha_{lc}\frac{\partial P}{\partial z}+Ap_{ilcg}\frac{\partial\alpha_{lc}}{\partial z}\\&-A\beta\alpha_g\alpha_{lc}\rho_m\left[\frac{\partial V_g}{\partial t}-\frac{\partial V_{lc}}{\partial t}+V_g\frac{\partial V_g}{\partial z}-V_{lc}\frac{\partial V_{lc}}{\partial z}\right]\\&=-A\Gamma_{lcv}(W_{icv}-V_{lc})+A\Gamma_d(V_{ld}-V_{lc})+A\tau_{icv}\\&-\chi_f C_l\frac{\rho_{lc}}{2}V_{lc}\mid V_{lc}\mid+A\alpha_{lc}\rho_{lc}g_z-R\frac{\alpha_g}{4}p_{ilcg}\frac{\partial A}{\partial z}\end{aligned}$$

Momentum balance of dispersed liquid field

$$\begin{aligned}&A\alpha_{ld}\rho_{ld}\left[\frac{\partial V_{ld}}{\partial t}+V_{ld}\frac{\partial V_{ld}}{\partial z}\right]+A\alpha_{ld}\frac{\partial P}{\partial z}+Ap_{ildg}\frac{\partial\alpha_{ld}}{\partial z}\\&=-A\Gamma_{ldv}(W_{idv}-V_{ld})+A\Gamma_a(V_{lc}-V_{ld})+A\tau_{idv}\\&+A\alpha_{ld}\rho_{ld}g_z\end{aligned}$$

Energy balance of gas field

$$\begin{aligned}&A\frac{\partial}{\partial t}\left(\alpha_g\rho_g\left[H_g+\frac{V_g^2}{2}\right]\right)+\frac{\partial}{\partial z}\left(A\alpha_g\rho_g V_g\left[H_g+\frac{V_g^2}{2}\right]\right)\\&-A\alpha_g\frac{\partial P}{\partial t}\\&=A(q_{vic}+q_{vid})+\chi_h q_{wv}+A\Gamma_{lcv}\left[H_v+\frac{W_{icv}^2}{2}\right]\\&+A\Gamma_{ldv}\left[H_v+\frac{W_{idv}^2}{2}\right]+A\alpha_g\rho_g V_g g_z\end{aligned}$$

Energy balance of continuous liquid field

$$\begin{aligned}&A\frac{\partial}{\partial t}\left(\alpha_{lc}\rho_{lc}\left[H_{lc}+\frac{V_{lc}^2}{2}\right]\right)+\frac{\partial}{\partial z}\left(A\alpha_{lc}\rho_{lc}V_{lc}\left[H_{lc}+\frac{V_{lc}^2}{2}\right]\right)\\&-A\alpha_{lc}\frac{\partial P}{\partial t}\\&=Aq_{lci}+\chi_h q_{wlc}-A\Gamma_{lcv}\left[H_{lc}+\frac{W_{icv}^2}{2}\right]\\&+A\Gamma_d\left[H_{ld}+\frac{V_{ld}^2}{2}\right]-A\Gamma_a\left[H_{lc}+\frac{V_{lc}^2}{2}\right]+A\alpha_{lc}\rho_{lc}V_{lc}g_z\end{aligned}$$

Energy balance of dispersed liquid field

$$\begin{aligned}&A\frac{\partial}{\partial t}\left(\alpha_{ld}\rho_{ld}\left[H_{ld}+\frac{V_{ld}^2}{2}\right]\right)+\frac{\partial}{\partial z}\left(A\alpha_{ld}\rho_{ld}V_{ld}\left[H_{ld}+\frac{V_{ld}^2}{2}\right]\right)\\&-A\alpha_{ld}\frac{\partial P}{\partial t}\\&=Aq_{ldi}+\chi_h q_{wld}-A\Gamma_{ldv}\left[H_{ld}+\frac{W_{idv}^2}{2}\right]\\&-A\Gamma_d\left[H_{ld}+\frac{V_{ld}^2}{2}\right]+A\Gamma_a\left[H_{lc}+\frac{V_{lc}^2}{2}\right]+A\alpha_{ld}\rho_{ld}V_{ld}g_z\end{aligned}$$

References

[1] J.G. Collier, Convective Boiling and Condensation, McGraw-Hill, New York, 1981.

[2] USSR Academy of Science Working Party of the Heat and Mass Transfer Section of the Scientific Council, Tubular data for calculating burnout when boiling water is uniformly heated round tubes, Thermal Eng. 23 (1977) 77–79.

[3] D.C. Groeneveld, S.C. Cheng, T. Doan, AECL-UO critical heat flux look-up table, Heat Transfer Eng. 7 (1986) 46–62.

[4] R.V. Macbeth, Burnout analysis, Part 5: examination of published world data for rod bundles, UKAEA Report no. AEEW-R358 (1964).

[5] Y. Katto, A generalized correlation of critical heat flux for the forced convective boiling in vertical uniformly heated round tubes, Int. J. Heat Mass Transfer 21 (1978) 1527–1542.

[6] H. Kumamaru, Y. Koizumi, K. Tasaka, Investigation of the pre- and post-dryout heat transfer of steam-water two-phase flow in a rod bundle, Nucl. Eng. Des. 102 (1987) 71–84.

[7] D. Bestion, The physical closure laws in the CATHARE code, Nucl. Eng. Des. 124 (1990) 229–245.

[8] D.C. Groeneveld, L.K.H. Leung, P.L. Kirillov, V.P. Bobkov, I.P. Smogalev, V.N. Vinogradov, X.C. Huang, E. Royer, The 1995 look-up table for critical heat fluxes in tubes, Nucl. Eng. Des. 163 (1996) 1–23.

[9] T.K.S Liang, C.J. Chang, H.J. Hung, Development of LOCA licensing calculation capability with RELAP5-3D in accordance with Appendix K of 10 CFR 50.46, Nucl. Eng. Des. 211 (2002) 69–84.

[10] P.B. Whalley, P. Hutchinson, G.F. Hewitt, The calculation of critical heat flux in forced convective boiling, in: Proceedings of 5th International Heat Transfer Conference, Tokyo, 1974, Paper no. B6.11.

[11] G.F. Hewitt, N.S. Hall-Taylor, Annular Two-phase Flow, Pergamon Press, Oxford, UK, 1970.

[12] G.F. Hewitt, A.H. Govan, Phenomenological modelling of non-equilibrium flows with phase change, Int. J. Heat Mass Transfer 33 (1990) 229–242.

[13] M. Naitoh, T. Ikeda, K. Nishida, T. Okawa, I. Kataoka, Critical power analysis with mechanistic models for nuclear fuel bundles, I: Models and verification for boiling water reactor applications, J. Nucl. Sci. Technol. 39 (1) (2002) 40–52.

[14] N. Hoyer, Calculation of dry out and post-dry out heat transfer for tube geometry, Int. J. Multiphase Flow 24 (1998) 319–334.

[15] C. Frepoli, L.E. Hochreiter, A.J. Ireland, K. Ivanov, Modelling of annular film dry out with COBRA-TF, in: 9th International Conference On Nuclear Engineering, ICONE-9, Lyon, France, 2001.

[16] M. Valette, S. Jayanti, Annular dispersed flow calculations with a two-phase three-field model, European Two-Phase Flow Group Meeting, Norway 12–13 May, 2003.

[17] S. Jayanti, M. Valette, Prediction of dry out and post-dry out heat transfer at high pressure using a one-dimensional three-fluid model, Int. J. Heat Mass Transfer 47 (2004) 4895–4910.

[18] V.P. Bobkov, V.N. Vinoradov, O.A. Zyatnina, N.V. Kozina, Considerations in describing burnout in rod bundles, Thermal Eng. 44 (3) (1997) 171–177.

[19] M. Lee, A critical heat flux approach for square rod bundles using the 1995 Groeneveld CHF table and bundle data of heat transfer research facility, Nucl. Eng. Des. 197 (2000) 357–374.

[20] A.W. Bennett, H.A. Kearsey, R.F.K. Keeys, Heat transfer to mixtures of high pressure steam and water in an annulus, Part VI: A preliminary study of heat transfer coefficient and heater surface temperature at high steam qualities, UKAEA Report no. AERE-R 4352 (1964).

[21] J. Wurtz, An experimental and theoretical investigation of annular steam-water flow in tubes and annuli at 30 to 90 bar, RISø Report no. 372 (1978).

[22] Y.A. Hassan, Predictions of vapour superheat in a rod bundle geometry with modified RELAP/MOD2, Trans. Am. Nucl. Soc. 54 (1987) 212–214.

[23] T.H. Chun, D.H. Hwang, W.P. Baek, S.H. Chang, Assessment of a tube-based bundle CHF prediction method using a subchannel code, Ann. Nucl. Energy 25 (14) (1998) 1159–1168.

[24] S. Sugawara, Y. Miyamoto, FIDAS: Detailed subchannel analysis code based on the three-fluid and three-field model, Nucl. Eng. Des. 120 (1990) 147–161.

[25] P. Knabe, F. Wehle, Prediction of dryout performance for boiling water reactor fuel assemblies based on subchannel analysis within the RINGS code, Nucl. Technol. 112 (1995) 315–323.

[26] N. Hoyer, M. Stepniewski, Dry out prediction in bundle geometry, in: Ninth International Topical Meeting on Nuclear Reactor Thermal Hydraulics (NURETH-9), San Francisco, California, USA, October 3–8, 1999.

[27] G.L. Yoder, D.G. Morris, C.B. Mullins, L.J. Ott, Dispersed flow film boiling heat transfer data near spacer grids in a rod bundle, Nucl. Technol. 60 (1983) 304–313, Also see NUREG/CR-2435, ORNL-5822.

[28] H. Kumamaru, Y. Koizumi, K. Tasaka, Critical heat flux for uniformly heated rod bundle under high-pressure, low-flow and mixed inlet conditions, J. Nucl. Sci. Technol. 26 (5) (1989) 544–557.

[29] D.A. Drew, R.T. Lahey, Application of general constitutive principles to the derivation of multi-dimensional two-phase flow equations, Int. J. Multiphase Flow 5 (1979) 243–264.

[30] S. Sugawara, Analytical prediction of CHF by FIDAS code based on three-fluid film-dry out model, J. Nucl. Sci. Technol. 27 (1990) 12–29.

[31] T. Ueda, M. Inoue, S. Nagatome, Critical heat flux and droplet entrainment rate in boiling of falling liquid films, Int. J. Heat Mass Transfer 24 (1981) 1257–1266.

[32] R.B. Bird, W.E. Stewart, E.N. Lightfoot, Transport Phenomena, Wiley, New York, 1960.

[33] K.M. Becker, C.H. Ling, S. Hedberg, G. Strand, An experimental investigation of post dry out heat transfer, Department of Nuclear Reactor Engineering, Royal Institute of Technology, KTH-NEL-33 (1983) Sweden.

[34] F. Barré, M. Parent, B. Brun, Advanced numerical methods for thermal hydraulics, Nucl. Eng. Des. 145 (1993) 147–158.